Naval Research Laboratory

Washington, DC 20375-5000

NRL Memorandum Report 6004

Variable Collision Frequency Effects on Hose and Sausage Instabilities in Relativistic Electron Beams

STEVEN P. SLINKER, RICHARD F. HUBBARD
AND MARTIN LAMPE

Plasma Theory Branch
Plasma Physics Division

August 12, 1987

A184 206

SECURITY CLASSIFICATION OF THIS PAGE

REPORT DOCUMENTATION PAGE

1a. REPORT SECURITY CLASSIFICATION UNCLASSIFIED	1b. RESTRICTIVE MARKINGS
2a. SECURITY CLASSIFICATION AUTHORITY	3. DISTRIBUTION / AVAILABILITY OF REPORT Approved for public release; distribution unlimited.
2b. DECLASSIFICATION / DOWNGRADING SCHEDULE	
4. PERFORMING ORGANIZATION REPORT NUMBER(S) NRL Memorandum Report 6004	5. MONITORING ORGANIZATION REPORT NUMBER(S)
6a. NAME OF PERFORMING ORGANIZATION Naval Research Laboratory 6b. OFFICE SYMBOL (If applicable) Code 4790	7a. NAME OF MONITORING ORGANIZATION Naval Surface Weapons Center
6c. ADDRESS (City, State, and ZIP Code) Washington, DC 20375-5000	7b. ADDRESS (City, State, and ZIP Code) Silver Spring, MD 20910
8a. NAME OF FUNDING / SPONSORING ORGANIZATION DARPA 8b. OFFICE SYMBOL (If applicable)	9. PROCUREMENT INSTRUMENT IDENTIFICATION NUMBER
8c. ADDRESS (City, State, and ZIP Code) Arlington, VA 22209	10. SOURCE OF FUNDING NUMBERS PROGRAM ELEMENT NO. 62707E PROJECT NO. N60921-85-WR-W0239 TASK NO. ARPA Order 4395, A54 WORK UNIT ACCESSION NO. DN680-415

11. TITLE (Include Security Classification)
Variable Collision Frequency Effects on Hose and Sausage Instabilities in Relativistic Electron Beams

12. PERSONAL AUTHOR(S)
Slinker, Steven P., Hubbard, Richard F. and Lampe, Martin

13a. TYPE OF REPORT	13b. TIME COVERED	14. DATE OF REPORT (Year, Month, Day)	15. PAGE COUNT
Interim	FROM _____ TO _____	1987 August 12	44

16. SUPPLEMENTARY NOTATION

17. COSATI CODES			18. SUBJECT TERMS (Continue on reverse if necessary and identify by block number)
FIELD	GROUP	SUB-GROUP	Beam propagation; Sausage instability; Hose instability; Collision frequency; Relativistic electron beam; Beam generated conductivity

19. ABSTRACT (Continue on reverse if necessary and identify by block number)

sub e nu sub m zeta

A relativistic electron beam propagating in a dense gas typically ionizes the gas weakly, and the resulting plasma conductivity evolution strongly influences beam stability properties. ~~We note in this paper that~~ the electric field E and the plasma electron temperature T_e usually decrease with distance ζ behind the beam head; as a result, the plasma electron-neutral collision frequency ν_m decreases with ζ, which depresses the conductivity σ in the front of the beam and increases σ further back in the beam. ~~We find that~~ this variation of ν_m, which has generally been ignored in previous models, substantially modifies beam instability evolution. Hose instability growth tends to increase very rapidly in the beam head and taper off to an asymptotic value for large ζ, in contrast to the pure power law growth seen when ν_m and $d\sigma/d\zeta$ are assumed to be constant. A second effect arises from local decreases in the perturbed conductivity σ_1 produced by perturbed electric field-driven increases in the local collision frequency. This destabilizing effect causes the beam to behave as if the mono-

sigma nu sub m zeta → next page

Sigma 1 d(sigma)/d(zeta)

(Continues)

20. DISTRIBUTION / AVAILABILITY OF ABSTRACT	21. ABSTRACT SECURITY CLASSIFICATION
☒ UNCLASSIFIED/UNLIMITED ☐ SAME AS RPT. ☐ DTIC USERS	UNCLASSIFIED
22a. NAME OF RESPONSIBLE INDIVIDUAL Steven P. Slinker	22b. TELEPHONE (Include Area Code) (202) 767-4792 22c. OFFICE SYMBOL Code 4792

DD FORM 1473, 84 MAR 83 APR edition may be used until exhausted. All other editions are obsolete. SECURITY CLASSIFICATION OF THIS PAGE

19. ABSTRACT (Continued)

pole conductivity (σ_θ) were replaced by $\sigma^* = \sigma_0 \left(1 - (E/\nu_m)\,(\partial\nu_m/\partial E)\right) \equiv \sigma_0(1 - \bar{q})$. Analytical models for the case of constant ($\bar{q}$) illustrate the pattern of rapid hose instability growth in the beam head followed by a "plateau" in hose amplitudes that is also observed in hose simulations with the VIPER model. The destabilizing effect of variable ν_m on the perturbed conductivity also occurs for the resistive sausage instability. However, the model calculation presented here shows that the threshold for sausage instability is not likely to be reached for reasonable beam and plasma parameters.

CONTENTS

VARIABLE COLLISION FREQUENCY EFFECTS ON HOSE AND SAUSAGE INSTABILITIES IN RELATIVISTIC ELECTRON BEAMS

I. INTRODUCTION

The resistive hose instability appears to be the dominant process leading to the observed disruption of propagation seen in many relativistic electron beam experiments.[1-4] In these experiments, the beam is injected into initially neutral gas, but beam ionization of the gas leads to a rapid rise in conductivity σ as the beam passes. A number of theoretical[5-7] and computational[7-13] models have been developed to study this instability, and the importance of the coupling between conductivity generation and beam dynamics has been realized for some time. If the plasma is weakly ionized, as is frequently the case, the plasma electron mobility is controlled by the collision frequency ν_m for momentum transfer between plasma electrons and neutral molecules. If ν_m is constant, σ is proportional to the plasma electron density n_e, independent of the plasma electron temperature T_e, and usually increases monotonically with distance $\zeta \equiv ct-z$ from the beam head. Lampe et al.[7] have shown that analytical dispersion relation estimates of the hose growth rate can be made if it is assumed that the beam and plasma current densities J_b and J_p, conductivity generation rate $d\sigma/d\zeta$, and beam relativistic factor γ are constant in ζ and z. The perturbed conductivity σ_1, tends to follow the perturbed beam current J_1, thus reducing the destabilizing repulsion in the "normal" case where J_p and J_b flow in opposite directions.

In the present paper, we discuss the effects due to the variation of ν_m with electron temperature T_e. Since T_e is typically controlled by ohmic heating and thus is a monotonically increasing function of the local electric field/gas density ratio E/ρ, one can also think of ν_m as a

Manuscript approved March 30, 1987

function of E/ρ alone. Furthermore, ρ is a constant for the cases considered in this paper, so ν_m can be regarded as a function of E. In most cases, T_e and E reach a peak at the "pinch point" in the expanded beam head and decrease with ζ in the well-pinched body and tail of the beam.[7-15] Since $\partial\nu_m/\partial T_e > 0$ for most weakly ionized gases and $\sigma = n_e e^2/m\nu_m$,[16-18] this causes conductivity to increase more rapidly with ζ after the pinch point than does n_e. Instability growth in ζ is characterized by the dipole decay length[5-7]

$$\zeta_1 = c\tau_1 = \frac{\pi\bar{\sigma}_o(\zeta)a^2}{2c} , \qquad (1)$$

where a is the beam scale radius and $\bar{\sigma}_o \equiv \sigma_o(r = 0)$. The combination of small n_e and large ν_m in the front of the beam can lead to very rapid hose instability growth in this region. However, the much larger n_e and smaller ν_m in the beam tail can cause hose growth rates to become quite small. As a result, the saturated transverse beam displacement $Y_{sat}(\zeta)$ can approach a constant value in the beam tail, contributing to the "plateau" behavior observed in many hose simulations.[9,11,13,14] In contrast, $Y_{sat}(\zeta)$ displays power law growth if $d\sigma/d\zeta$ and ν_m are assumed to be constant.[5,7]

This paper will also discuss a destabilizing mechanism associated with the perturbed conductivity[7] σ_1 when $\partial\nu_m/\partial E > 0$ or $\partial\nu_m/\partial T_e > 0$. As pointed out previously, σ_1 reduces instability growth when ν_m is constant because the local conductivity and electron density increase in regions where the distortion associated with the instability increases the beam density. However, the electric field $|E_z|$ also increases in such regions, thus increasing ν_m and decreasing σ. This results, in some cases, in a substantial increase in hose growth.[13] If ν_m is assumed to be a function of E/ρ only, we shall show that the monopole (unperturbed) conductivity in the perturbed Ampere's law can be replaced by

$$\sigma^* = \sigma_o \left(1 - \frac{E}{\nu_m} \frac{\partial \nu_m}{\partial E}\right) \equiv \sigma_o(1 - \bar{q}). \qquad (2)$$

Since $\bar{q}$ can exceed 0.5 for air, hose growth rates can be substantially increased. This destabilizing mechanism competes with the stabilizing effect of perturbed conductivity described by Lampe et al.[7] Equation (2) represents one of the major results of this study.

In Sec. II of this paper we derive equations for the perturbed conductivity and fields when ν_m is a function of E. Specializing further, we obtain analytic solutions for beam equilibrium and hose instability for the case with constant $dn_e/d\zeta$ and ν_m proportional to E^q (with q constant). Hose simulation results obtained with the VIPER multi-component simulation model[7] are described in Sec. III. A sausage instability model using the assumptions in Sec. II is presented in Sec. IV, showing that the destabilizing effects of the variable collision frequency are not strong enough except in extreme cases to give significant instability growth. The implications of this study are discussed in the final section.

II. THEORETICAL CONSIDERATIONS

A. Introduction

In this section, we will derive some simple models which illustrate some of the important effects of variable ν_m conductivity on hose instability. Much of this work is a direct extension of the calculations of Lampe et al.[7] with constant ν_m. The spread mass beam dynamics model[5] will be employed since that model leads to tractable dispersion relations in some situations.

B. Conductivity and Momentum Transfer Frequency

We consider the case in which the beam propagates in a resistive medium which has a scalar conductivity given by

$$\sigma = \frac{n_e e^2}{m\nu_m}. \tag{3}$$

Many physical processes contribute to the determination of $\sigma(\underset{\sim}{x},t)$, and a variety of theoretical models, both simple and complex, have been used. The electron density n_e is determined by beam-collisional ionization, avalanche ionization, recombination, and attachment. However, we shall concentrate on the "beam body" region where collisional ionization dominates, and n_e is given by

$$\frac{dn_e}{d\zeta} = \mu J_b, \tag{4}$$

where μ is the production rate due to beam impact ionization and J_b is the beam current density. Theoretical models are available to prescribe the collision frequency ν_m as a function of T_e. If, for example, the electron distribution function f(v) is approximately isotropic with a temperature T_e, then ν_m is given by

$$\frac{1}{\nu_m(T_e)} = -\frac{4\pi}{3n_e}\int \frac{v^3}{\sum_i v\sigma_{mi}M_i}\frac{\partial f}{\partial v}\,dv \qquad (5)$$

where $\sigma_{mi}(E)$ is the momentum transfer cross section for electron collisions with a species i with number density M_i.[19] For a Maxwellian f(v), Slinker and Ali[17] have compiled tables of $\nu_m(T_e)$ for N_2 and O_2 based on Eq. (5). Figure 1 shows $\nu_m(T_e)$. Alternatively, ν_m may be deduced from drift velocity measurements in discharges,[20,21] in which case, ν_m is known as a function of the electric field/gas density ratio E/ρ. Over a wide range of validity T_e may be expressed as a function of E/ρ, so that ν_m may in any case be regarded as a function of E/ρ. Electron heating is usually dominated by ohmic heating and direct deposition by the beam, while collisions with neutrals result in electron cooling through vibrational and electronic excitations.[21] Thus

$$\frac{\partial T_e}{\partial t} = \left(\frac{2}{3}\varepsilon_s - T_e\right)\frac{S_B}{n_e} + \frac{2}{3}\frac{\sigma E^2}{C_{ev}n_e} - \frac{2}{3}n_n R_n(T_e), \qquad (6)$$

where $C_{ev} = 1.6\times10^{-12}$ergs/eV, S_B is the production rate due to beam impact ionization, ε_s is the average energy of a secondary electron ($\simeq$ 7.55 eV for air), and $R_n(T_e)$ is the cooling rate due to collisions with neutrals with density n_n. If $\partial T_e/\partial t \simeq 0$, and ohmic heating balances excitation cooling, then T_e is a function of E/ρ only. [This follows from the fact that $\sigma = (n_e/\rho)\times$(function of T_e) for weakly ionized gas.] Thus ν_m can be expressed as a function of E/ρ.

C. Linearized Conductivity and Field Equations

The hose instability is usually treated analytically by partitioning J_b, σ, E_z, etc., into monopole (m = 0) and dipole (m = 1) quantities,[5-7] and linearizing in the dipole quantities, which are treated as small perturbations about axi-symmetry. For example,

$$\sigma(r,\zeta,z,\theta) = \sigma_o(r,\zeta,z) + \sigma_1(r,\zeta,z)\cos\theta. \tag{7}$$

We will use the 0 and 1 subscripts to denote unperturbed (m = 0) and perturbed (m = 1) quantities. In the absence of avalanche and recombination processes the electron density is given by

$$\frac{dn_{eo}}{d\zeta} = \mu J_{bo} \tag{8a}$$

$$\frac{dn_{e1}}{d\zeta} = \mu J_{b1}. \tag{8b}$$

If ν_m is a function of E/ρ and ρ is constant, then

$$\sigma_o = \frac{n_{eo}e^2}{m\nu_m(E)} \tag{9a}$$

$$\sigma_1 = \frac{n_{e1}e^2}{m\nu_m(E)} - \frac{n_{eo}e^2}{m\nu_m^2}\left(\frac{\partial\nu_m}{\partial E_o}\right)E_1$$

$$= \sigma_o\left(\frac{n_{e1}}{n_{eo}} - \frac{E_1}{\nu_m}\frac{\partial\nu_m}{\partial E_o}\right). \tag{9b}$$

The paraxial beam approximation is made,[5] and the conductivity is assumed to be sufficiently large to provide space charge neutrality, so that $E_r = 0$. Then A_z becomes the only significant component of the vector potential,[5]

$$E_o \equiv E_{zo} = - \frac{\partial A_o}{\partial \zeta} \tag{10a}$$

$$E_1 \equiv E_{z1} = - \frac{\partial A_1}{\partial \zeta} , \tag{10b}$$

and Maxwell's equations reduce to Ampere's law,

$$\left(\frac{1}{r} \frac{\partial}{\partial r} r \frac{\partial}{\partial r} - \frac{4\pi\sigma_o}{c} \frac{\partial}{\partial \zeta}\right) A_o = - \frac{4\pi}{c} J_{bo}, \tag{11a}$$

$$\left(\frac{\partial}{\partial r} \frac{1}{r} \frac{\partial}{\partial r} r - \frac{4\pi\sigma_o}{c} \frac{\partial}{\partial \zeta}\right) A_1 = - \frac{4\pi}{c} J_{b1} + \frac{4\pi\sigma_1}{c} \frac{\partial A_o}{\partial \zeta} . \tag{11b}$$

Using (9b) for σ_1 and (10) for E_o and E_1, Eq. (11b) can be rewritten as

$$\left[\frac{\partial}{\partial r} \frac{1}{r} \frac{\partial}{\partial r} r - \frac{4\pi\sigma_o}{c} \left(1 - \frac{E_o}{\nu_m} \frac{\partial \nu_m}{\partial E_o}\right) \frac{\partial}{\partial \zeta}\right] A_1 = - \frac{4\pi}{c} \left(J_{b1} + \sigma_o E_o \frac{n_{e1}}{n_{eo}}\right). \tag{12}$$

Equation (12), supplemented by Eq. (8b), specifies the perturbed potential A_1 in terms of the perturbed beam current J_{b1}. It is formally similar to Eq. (9) of Ref. 7, which was derived for the case of constant ν_m. The effects of beam-generated perturbed conductivity σ, appear in two places -- the last term on the right-hand side (the "density term") and the last term on the left-hand side (the "field term"). The density term has been discussed previously.[7] For the usual case in which the plasma current J_p is a return current flowing opposite to J_b, the density term is stabilizing; it leads to conductivity perturbations which follow the beam distortions and thus tend to reduce the spatial separation between beam and plasma currents. The "field term", which is discussed for the first time in this paper, does not change the mathematical structure of the equation, but in essence replaces the conductivity $\sigma_o(\zeta)$ on the left-hand side by an effective conductivity

$$\sigma^* \equiv \sigma_o\left(1 - \frac{E_o}{\nu_m}\frac{\partial \nu_m}{\partial E_o}\right) \equiv \sigma_o(1-\bar{q}), \qquad (13)$$

where σ^*, σ_o, ν_m, E_o and $\bar{q}$ are, in general, functions of ζ, z, and r. Similarly, the dipole decay length τ_1, the characteristic length scale for instability growth in ζ, is replaced by an effective value,

$$\tau_1^* \equiv \pi\sigma^*(r=0)a^2/2c^2 \equiv (1-\bar{q})\tau_1. \qquad (14)$$

For "normal" weakly ionized gases such as air, $0 < \bar{q} < 1$. Thus the $(1-\bar{q})$ term reduces τ_1^* and increases the instability growth rate. One must also note, however, that the dependence of ν_m on E_o also directly modifies σ_o in Eqs. (12) and (13). In propagating beams, E_o steadily decreases, as a function of ζ, from a maximum at the "pinch point" just behind the beam head.[22] Thus, in "normal" gases ν_m is a decreasing function of ζ, which tends to augment the increase of σ_o as a function of ζ. This term thus acts to speed up hose growth near the front of the beam and slow it down further back in the beam.

In the next sections we shall derive explicit solutions of Eqs. (8), (12), and the equations for beam dynamics that illustrate these effects.

D. Analytic Solutions for Beam Equilibrium

A number of previous works[5-7] have derived analytic solutions for hose growth by introducing some additional simplifications and assumptions in the assumed equilibrium and the beam dynamics. This has proven quite useful, particularly for developing insight into instability growth and scaling. In this section, we shall calculate beam equilibria, adopting the familiar assumptions used in these earlier works, but concentrating on the new effects introduced by variable ν_m. In the next section we shall use the same assumptions to calculate hose growth analytically.

We assume that the beam current I_b is constant, and that the beam equilibrium current density J_{bo} has a Bennett radial profile,

$$J_{bo}(r) = \frac{I_b/\pi a^2}{(1+r^2/a^2)^2} \equiv \frac{\bar{J}_{bo}}{(1+r^2/a^2)^2}, \qquad (15)$$

where the Bennett radius a is constant. Lee[23] has shown that, under certain conditions, beams evolve toward the Bennett profile as a result of scattering, and this has also been observed experimentally.[23,24] The assumption of constant Bennett radius is reasonable in the beam body. It follows from Eq. (8a) that n_{eo} also has a Bennett profile in the beam body. An approximate solution of Eq. (11a) is then given by

$$A_o(r,\zeta) = \bar{A}_o(\zeta) \ln\left(\frac{1+r^2/a^2}{1+R_o^2/a^2}\right), \qquad (16a)$$

where $\bar{A}_o(\zeta)$ satisfies

$$\bar{A}_o(\zeta) + \frac{\pi a^2 \bar{n}_o e^2}{mc\nu_m} \ln\left(1 + \frac{R_o^2}{a^2}\right) \frac{d\bar{A}_o}{d\zeta} = -\frac{\pi a^2}{c} \bar{J}_{bo}, \qquad (16b)$$

and R_o is a radius (usually $R_o >> a$)[5-7] where A_o goes to zero. $\bar{J}_{bo}$ and $n_o = \mu \bar{J}_{bo} \zeta$ are the axis values, independent of r. The approximation made in going from (11a) and (16a) to (16b) is to neglect the weak logarithmic dependence of $E_z \equiv -\partial A_o/\partial\zeta$ on r; this also results in the plasma current density $J_{po}(r,\zeta)$ having a Bennett radial profile with $J_{po}(0,\zeta) \equiv \bar{J}_p(\zeta)$.

We assume additionally that

$$\nu_m(E) = \beta |E|^q, \qquad (17)$$

where β and q are constants. Thus, the correction factor $\bar{q}$ in (13) or (14) is constant and equal to q. For many gases, this is a good assumption over a wide range of values of E/ρ (with ρ constant). However, it must be

remembered that if $|E|$ becomes very large, avalanche breakdown will occur, thus invalidating Eqs. (8) and (17). If, on the other hand, $|E|$ becomes very small, the temperature T_e will depend on processes other than ohmic heating, the full Eq. (6) must be used, and ν_m will become independent of E.

Having made these assumptions, Eq. (16b) can be rewritten as

$$-\bar{A}_o(\zeta) + \kappa\zeta \left(-\frac{d\bar{A}_o}{d\zeta}\right)^{1-q} = \frac{\pi a^2}{c} \bar{J}_{bo}, \tag{18}$$

where

$$\kappa = \frac{\pi a^2 \mu \bar{J}_{bo} e^2}{mc\beta} \left[\ln\left(1 + \frac{R_o^2}{a^2}\right)\right]^{1-q}, \tag{19}$$

where we have also used the fact that

$$\frac{d\bar{A}_o}{d\zeta} < 0, \tag{20}$$

if $\bar{J}_{bo} > 0$. For constant $\bar{J}_{bo}$ and $\bar{A}_o(\zeta_o) = 0$, Eq. (18) has the solution

$$\bar{A}_o(\zeta) = -\frac{\pi a^2}{c} \bar{J}_{bo}\left(1 - \left(\frac{\zeta_o}{\zeta}\right)^{1/\kappa}\right) \tag{21a}$$

if $q = 0$, or

$$\bar{A}_o(\zeta) = -\frac{\pi a^2}{c} \bar{J}_{bo} + \left[\left(\frac{\pi a^2}{c} \bar{J}_{bo}\right)^{-\frac{q}{1-q}} \kappa^{-\frac{1}{1-q}} \left(\zeta^{-\frac{q}{1-q}} - \zeta_o^{-\frac{q}{1-q}}\right)\right]^{-\frac{1-q}{q}} \tag{21b}$$

if $q \neq 0$ and $q \neq 1$. We are assuming $\zeta > \zeta_o$.

We may now consider the general nature of this equilibrium for various ranges of q.

Case (i): $q < 0$. A singularity exists at some finite value ζ^* of ζ, where $\bar{A}_o \to -(\pi a^2 \bar{J}_{bo}/c)$, $E_o \to 0$, $\sigma_o \to 0$, and $\bar{J}_{po} \to 0$. For $\zeta > \zeta^*$, the only solution is $E_o = \bar{\sigma}_o = \bar{J}_{po} = 0$. This singularity occurs because Eqs. (3) and (17) specify that σ goes to zero for $E \to 0$. It is unphysical, of course; Eq. (17) loses its validity when $|E|$ becomes small. However, it can be shown that the plasma current density $\bar{J}_{po}$ decreases from its initial value on a ζ scale that is slow compared to the scale length for hose growth essentially because of the large quantity $\ln(1 + R_o^2/a^2)$ in the definition of κ, Eq. (19). Thus, there is a range of ζ where it can be assumed that $\bar{J}_{po}$ is constant which will be seen to simplify the instability calculation.

Case (ii): $q = 0$. This case is well known. Here $E_o \sim \zeta^{(-1/\kappa-1)}$, $\bar{\sigma}_o \sim \zeta$, and $\bar{J}_p \sim \zeta^{-1/\kappa}$. The plasma current decays to zero as $\zeta \to \infty$, but again, this decay is slow compared to the ζ scale for hose growth.

Case (iii): $0 < q < 1$. Here $E_o \sim \zeta^{-1/1-q}$, $\bar{\sigma}_o \sim \zeta^{1/1-q}$, and $\bar{J}_{po} \to$ const as $\zeta \to \infty$. This scaling eventually breaks down at large ζ: either $|E|$ becomes so small that Eq. (17) becomes invalid, or alternatively, recombination may become important in limiting n_{eo}, in which case Eq. (8a) becomes invalid. In either case, $\bar{J}_{po}$ eventually decays to zero asymptotically at $\zeta \to \infty$. However, it is reasonable once again to assume that $\bar{J}_{po}$ is constant over the ζ scale for hose growth.

Case (iv): $1 < q$. This case is very peculiar, since the effective conductivity σ^* is negative. If a current J_{po} is flowing in the gas, small local increases in $|E|$ decrease the current! Gases do exist which have this property for certain ranges of E/ρ. Christophorou[26] gives several examples, such as argon doped with C_2H_2. Current flow is unstable in such a gas, even in the absence of an electron beam, since the left-hand side of Eq. (12) is a diffusion equation with a negative diffusion coefficient. It

is thus clear that one cannot assume simple equilibria of the type considered here. We shall not consider this case further.

E. Analytic Solution for Hose Growth

1. Conductivity and Field Equations

As we have seen in the previous subsection, if $q < 1$ it is qualitatively reasonable to assume that $\bar{J}_{po}$ is constant over the ζ scale of primary interest for hose growth. (However, we must keep in mind that eventually $\bar{J}_{po}$ does decay to zero as $\zeta \to \infty$.) Making this assumption, in addition to those discussed previously, significantly simplifies the hose growth problem. We shall define a current neutralization fraction $f \equiv \bar{J}_{po}/\bar{J}_{bo}$ which is a constant. Equation (8a) reduces to

$$n_{eo} = \mu J_{bo} \zeta, \tag{22}$$

and the density term in the perturbed conductivity in (12) is

$$\sigma_o E_o \frac{n_{e1}}{n_{eo}} = \frac{f J_{bo} n_{e1}}{\mu J_{bo} \zeta} = \frac{f n_{e1}}{\mu \zeta}. \tag{23}$$

Following Ref. 7, we take

$$\frac{\partial n_{e1}}{\partial \zeta} = \left(1 + \zeta \frac{\partial}{\partial \zeta}\right) \frac{n_{e1}}{\zeta} = \mu J_{b1}. \tag{24}$$

Thus, Ampere's Law (12) takes the form

$$\left(1 + \zeta \frac{\partial}{\partial \zeta}\right)\left(\frac{\partial}{\partial r} \frac{1}{r} \frac{\partial}{\partial r} r A_1 - \frac{4\pi}{c} \sigma_o \left(1-q\right) \frac{\partial A_1}{\partial \zeta}\right)$$

$$= - \frac{4\pi}{c}\left(1 + \zeta \frac{\partial}{\partial \zeta} + f\right) J_{b1}. \tag{25}$$

Equation (25) is identical to (13) in Ref. 7 if one replaces $K J_{bo} \zeta$ with $\sigma_o(1-q) = \sigma_o^*$.

2. Spread Mass Hose Instability Model

In order to estimate hose instability amplitudes, the field equation (25) must be combined with a beam dynamics model which specifies J_{b1} in terms of A_1. Following Ref. 7 we assume that perturbed quantities have a z-dependence $\exp(-i\Omega z)$ and employ the spread mass model of Lee.[5] In this model, the perturbed current and vector potential are assumed to be rigid displacements of the equilibrium profiles: $J_{b1} = -Y(dJ_{bo}/dr)$ and $A_1 = -D(dA_o/dr)$. The displacements Y and D are related by

$$Y(\zeta) = D(\zeta)\left(1 + G(s)\right), \tag{26}$$

where $s \equiv \Omega^2/\Omega_{\beta o}^2$, $\Omega_{\beta o} \equiv [2\pi(1 + f)eJ_{bo}(0)/(\gamma mc)]^{1/2}$ is the on-axis betatron frequency, and G(s) is Lee's spread mass weighting function[5] which for a Bennett profile is

$$G(s) = 6s\left\{\frac{1}{2} - s + (s - s^2)\left[\pi i + \ln\left(\frac{1+s}{s}\right)\right]\right\}. \tag{27}$$

Inserting these relationships into (25) along with the equilibrium and perturbed radial dependences for J_b, σ, and A results in the following ordinary differential equation for the field displacement $D(\zeta)$

$$\left(1 + \zeta\frac{d}{d\zeta}\right)\left(1 + \lambda_q(1-q)\zeta^{\frac{1}{1-q}}\frac{d}{d\zeta}\right)D = \frac{(1+G(s))}{(1+f)}\left(1 + f + \zeta\frac{d}{d\zeta}\right)D, \tag{28}$$

where the constant λ_q is

$$\lambda_q = \frac{\pi\mu' I_b}{2c}\left(\frac{|f|}{\mu'}\right)^{\frac{-q}{1-q}}, \tag{29}$$

with $\mu' = e^2\mu/m\beta$.

We assume that $\nu_m \sim E^q$, so that

$$\sigma_o(\zeta) = \frac{2c}{\pi a^2} \lambda_q \zeta^{\frac{1}{1-q}}. \qquad (30)$$

Equation (28) reduces to the result in Ref. 7 for q = 0; in that case, a dispersion relation can be obtained by replacing ζ by ln ζ as the independent variable. In the present case, it is not possible to derive a dispersion relation in closed form, but the hose growth resulting from Eq. (28) can be expressed in terms of tabulated functions or calculated by numerical integration.

3. Kummer Function Solutions

The solution to Eq. (28) can be expressed purely analytically in terms of confluent hypergeometric functions. Although not very useful for obtaining numerical results, this method can illuminate some of the analytical properties of the instability for large ζ in different ranges of q.

Equation (28) can be rewritten as Kummer's equation,[25]

$$w \frac{d^2D}{dw^2} + (b - w) \frac{dD}{dw} - aD = 0 \qquad (31)$$

by changing variables to

$$w = \left(- \frac{1}{\lambda_q q} \frac{G-f}{1+f} \right) \zeta^{- \frac{q}{1-q}}. \qquad (32)$$

Here the coefficients are

$$a = \left(\frac{1-q}{q} \right) \frac{(1+f)G}{f-G}, \qquad (33)$$

$$b = \frac{1-q}{q}. \qquad (34)$$

The solutions are the Kummer's functions M(a,b,w) and U(a,b,w) with arguments defined by (32), (33) and (34). The complete solution is

$$D(\zeta(w)) = AM(a,b,w) + BU(a,b,w), \qquad (35)$$

with A and B arbitrary constants.

For $0 < q < 1$, which is the range of interest for weakly ionized air, the limit $\zeta \to \infty$ corresponds to $w \to 0$. In this limit, we have

$$D(w=0) = A + B\,\frac{\Gamma(1-b)}{\Gamma(1+a-b)} = \text{constant}. \qquad (36)$$

This implies that the hose amplitudes in the beam tail approach a finite asymptotic limit as $\zeta \to \infty$, in contrast to the case of $q = 0$, where it was found in Ref. 7 that $D(\zeta) \sim \zeta^{\omega_i}$ and is unbounded. In principle, it is possible to give an analytical estimate of this bound by first assuming that at $w = 0$, $D = 1$ and $dD/dw = 0$ to get A and B. One can then assume that growth begins at a point ζ_o which is sufficiently small that $w(\zeta_o) \equiv w_o >> 1$. Then using the asymptotic expansions for $M(a,b,w_o)$ and $U(a,b,w_o)$ gives

$$D(w_o) = A\left\{\frac{\Gamma(b)}{\Gamma(b-a)}\, e^{\pm i\pi a} w_o^{-a} + \frac{\Gamma(b)}{\Gamma(a)}\, e^{w_o} w_o^{a-b}\right\} + B\, w_o^{-a}. \qquad (37)$$

The ratio of hose displacements is then given by

$$\frac{D(\zeta \to \infty)}{D(\zeta_o)} = \frac{D(w \to 0)}{D(w_o)}. \qquad (38)$$

Since G(s) is complex, w is in general complex, so numerical solutions to (36-38) are not easy to obtain. It is easier to simply integrate (28) numerically, as discussed in the next subsection. Even though the hose amplitudes have a finite limit, in most cases of interest $D(\zeta \to \infty) >> D(\zeta_o)$, so that substantial hose growth occurs.

Solution for q in other ranges can also be obtained. For q = 0, the transformation is invalid, but this case has already been worked out in Ref. 7. For q = 1, the effective conductivity $\sigma^* \to 0$, and the instability is absolute. The case q < 0 corresponds to having ν_m decrease with E, as is the case in the Spitzer conductivity regime. In this case, b ranges from $+\infty$ (for $q \to 0^-$) to 1 for $q \to -\infty$. Then $\zeta \to \infty$ corresponds to $w \to \infty$, and the solutions are (Ref. 22, Eqs. 13.5.1 - 13.5.2):

$$D(\infty) \simeq A \left\{ \frac{\Gamma(b)}{\Gamma(b-a)} e^{\pm i\pi a} w^{-a} + \frac{\Gamma(b)}{\Gamma(a)} e^{w} w^{a-b} \right\} + B w^{-a}. \qquad (39)$$

The second term is unbounded if $\mathrm{Re}[G(1+f)/(f-G)] < 0$, resulting in unlimited hose growth. This condition is usually satisfied.

4. Direct Numerical Integration

Since the purely analytical solutions described above are cumbersome, it is perhaps more useful to integrate the field displacement equation (28) numerically. This requires an appropriate choice for the starting point ζ_o and the constant λ_q. For q = 0, Lampe et al.[7] used

$$\lambda_{q=0} \equiv \lambda_o = .044\ I_b(\mathrm{kA}), \qquad (40)$$

and estimated the return current fraction

$$f = \frac{-\lambda_o \eta_f}{1+\lambda_o \eta_f}$$

with $\eta_f \simeq 1$.

In order to compare results with different values of q, we assume a value of λ_o and require that at a reference point ζ_N, the dipole decay length is equal to the nominal q = 0 value, $\lambda_o \zeta_N$. Combining (1), (14), and (30) results in

$$c\tau_1 = \frac{\lambda_q \zeta^{\frac{1}{1-q}}}{1-q}. \qquad (42)$$

Thus, the value of λ_q which gives $c\tau_1(\zeta_N) = \lambda_o \zeta_N$ is

$$\lambda_q = (1-q)(\lambda_o \zeta_N)\zeta_N^{-\frac{1}{1-q}} = (1-q)\lambda_o \zeta_N^{\frac{-q}{1-q}}. \qquad (43)$$

The starting point ζ_o for the perturbation is arbitrarily chosen to be the point at which $c\tau_1(\zeta_o) \simeq a_o$, the nominal beam radius. Given λ_q from (43), ζ_o can be calculated from (42) for any chosen value of $c\tau_d(\zeta_o)$. Finally, initial values for $D_o \equiv D(\zeta_o)$ and $dD(\zeta_o)/d\zeta$ must be chosen; we have assumed Re D_o = Im D_o = $\sqrt{2}/2$ and $dD(\zeta_o)/d\zeta = 0$.

An example of hose instability growth for various values of q is shown in Fig. 2. The following parameter values were chosen: $\eta_f = 1$, $\lambda_o = 1$, $\zeta_N = 20\ a_o$, $f = -0.5$, $\Omega_r/\Omega_{\beta o} = 0.5$, and $c\tau_1(\zeta_o) = a_o$. For $q = 0$, pure power law growth is observed for $\zeta \gtrsim 10\ a_o$ with a slope equal to the value $\bar{\omega}_i = 1.80$ predicted by the dispersion relation of Ref. 7. For $q = 0.50$, hose growth is very rapid in the front of the beam but flattens out into a plateau for $\zeta \gtrsim 100\ a_o$. This qualitative behavior is seen for a wide range of λ_o values and becomes more pronounced as q approaches 1.

III. HOSE INSTABILITY SIMULATIONS WITH VARIABLE ν_m MODELS

A. Introduction

The hose growth behavior shown in Fig. 2 has been observed in a variety of simulation models including VIPER,[7,13] SIMM1,[10] SARLAC,[14] EMPULSE,[9] and PHLAP.[11] These codes allow J_b, J_p, and n_e to vary with r, ζ, and z and permit J_b, J_p, and σ to have different radial profiles. In this section, results from the VIPER multi-component simulation model will be presented for cases with $\nu_m = \nu_m(E/\rho)$. A description of the VIPER model and some examples with a fixed ν_m conductivity model are contained in Ref. 7.

B. VIPER Simulation With $\nu_m \sim E^q$

The case described in Sec. II can be simulated by using a momentum transfer frequency of the form

$$\nu_m(E/\rho) = \nu_m^o + \nu_m^1(E/\rho)^q. \qquad (44)$$

The floor on ν_m is used to avoid unrealistically large conductivity in the weak field regions of the beam. Avalanche, recombination, and beam expansion due to scattering have been turned off in the simulation, but J_p and J_b do vary with z and ζ. The principal quantity of interest is $Y_{sat}(\zeta)$, the maximum or "saturated" displacement of the beam slice at a distance ζ from the beam head as it propagates forward in z.

Figure 3 plots $Y_{sat}(\zeta)$ for a series of VIPER simulations in which the exponent q in (44) was varied. The initial perturbation began at $\zeta_o = a_o$, and ν_m^1 was chosen to give a reference momentum transfer frequency of $1.4 \times 10^{12} sec^{-1}$ at $E/\rho = 3$ kV/cm-atm. As q is increased, $Y_{sat}(\zeta)$ shows the qualitative behavior seen in Fig. 2. Higher values of q give more pronounced plateau behavior.

C. VIPER Simulations With More Elaborate Conductivity Model

A more elaborate conductivity model,[18] based on rate equations and $\nu_m(T_e)$ calculations from Slinker and Ali[17] and Ali,[21] has also been used with VIPER. The model assumes a $T_e(E/\rho)$ relation deduced by Ali:[21]

$$T_e = T_{eo} + 0.1(E/\rho)^{0.8} \qquad (45)$$

with E/ρ in volts/cm-torr, T_e in eV, and $T_{eo} = 0.15$ eV. The total collision frequency is the sum of ν_m and the electron-ion contribution.

Figure 4 shows the maximum hose displacement (saturation had not occurred by the time of the graph) as a function of ζ for a 10 kA, 5 mm beam. The three curves correspond to three VIPER runs. In A, the full dipole conductivity terms in (9b) are retained. In B, the dipole conductivity is set equal to zero. In C, only the contribution to σ_1 due to n_{e1} is retained. As seen in the figure, this part of the dipole conductivity is stabilizing.[7] The inclusion of the $\partial\nu_m/\partial E_o$ term, Case A, is seen to be destabilizing in accordance with theory.

Finally, Fig. 5 shows the on-axis conductivity, $\bar{\sigma}$, electric field and fraction $\bar{\sigma}^*/\bar{\sigma}$ as a function of ζ. Since most of the hose growth occurs in the region $50 < \zeta/a_o < 300$ where $\bar{\sigma}^*/\bar{\sigma} \tilde{=} 0.6$ is approximately constant, Eq. (12) suggests that lnY(Case C)/lnY(Case A) should be approximately 0.6. Figure 4 confirms this expectation.

IV. SAUSAGE INSTABILITY FOR $\nu_m \sim E^q$

A. Introduction

The resistive sausage instability is excited by the repulsive force between the beam current and return current. This is an axisymmetric ($m = 0$) mode in which the beam expands or contracts self-similarly. For an infinite beam with constant conductivity, the instability is excited when the ratio $-I_p/I_b = -f$ exceeds 0.69 for a Bennett profile.[28] However, the instability to our knowledge has never been unambiguously observed in simulations or experiments in which beam impact ionization is the dominant conductivity generation mechanism.

Lampe and Joyce[28] have shown that for the assumptions used in Section III (f, J_{bo}, and $d\sigma_o/d\zeta$ constant), and if in addition $q = 0$, the inclusion of dipole conductivity effects leads to the following instability threshold condition on the return current fraction f:

$$\eta_f = \frac{-f}{1+f} > \frac{(2\lambda_o + \sqrt{3})^2}{\lambda_o + 1} H(\alpha, \lambda_o). \qquad (46)$$

The function $H(\alpha, \lambda_o)$ is a slowly varying function which approaches 0.8 when the anharmonic damping coefficient, α, equals Lee's[29] value of 0.7, and $H(\alpha \to \infty, \lambda_o) \to 1$. If one estimates f from (41), the instability condition is not reached unless $\eta_f \gtrsim 4$, a situation almost never observed in beam simulations. Thus, Lampe and Joyce[28] concluded that the sausage instability should be stabilized in almost all conceivable cases for beams propagating in initially neutral gases.

In the next section, we extend the analysis of Ref. 28 to the case where $\nu_m \sim (E/\rho)^q$. This introduces the destabilizing dipole conductivity term in Ampere's Law (12) and reduces the threshold return current fraction $|f|$.

B. Derivation of Sausage Dispersion Relation

Lampe and Joyce[28] used an envelope equation approach to treat the linearized sausage instability. The perturbed beam and plasma currents δJ_b and δJ_p are assumed to have the form

$$\delta J = - \tilde{J}(\zeta,z) \frac{1-r^2/a_o^2}{[1+r^2/a_o^2]^3} \tag{47a}$$

and the perturbed vector potential is given by

$$\delta A = - \tilde{D}(\zeta,z) \frac{1-r^2/a_o^2}{1+r^2/a_o^2}. \tag{47b}$$

The unperturbed conductivity is given by (9a), and the perturbed conductivity has the radial dependence given in Eq. (19) of Lampe and Joyce.[28] The perturbed envelope equation can be written as

$$\bar{\Omega}_\beta^2 \frac{\partial^2 \tilde{J}_b}{\partial z^2} = - \alpha \bar{\Omega}_\beta \frac{\partial \tilde{J}_b}{\partial z} - \left(2 + \left(\frac{2}{3}\right) \frac{f}{1+f}\right) \tilde{J}_b + \frac{(2/3)\tilde{J}_p}{1+f}, \tag{48}$$

where we have changed the notation from that of Ref. 25 to be consistent with the rest of this paper. The average betatron frequency $\bar{\Omega}_b = \Omega_{\beta o}/\sqrt{2} = a_o^{-1}(I_b(1+f)/I_A)^{1/2}$ where $I_A = \gamma mc^3/e$ is the Alfven current.

Using the assumed radial dependence for the various quantities in Ampere's Law results in

$$\left(1 + \zeta \frac{\partial}{\partial \zeta}\right) \tilde{J}_p = f\tilde{J}_b - \left(1 + \zeta \frac{\partial}{\partial \zeta}\right) \sigma_o(r=0)(1-q) \frac{\partial \tilde{D}}{\partial \zeta}. \tag{49}$$

To close the system, we note that

$$\tilde{D} = \frac{\pi a_o^2}{2c} \left(\tilde{J}_b + \tilde{J}_p\right), \tag{50}$$

and Fourier analyze in z, assuming a z-dependence $\exp(-i\hat{\Omega}\bar{\Omega}_\beta z)$. This gives

$$\tilde{J}_b = \frac{\frac{2}{3}(1+f)^{-1}\tilde{J}_p}{-\hat{\Omega}^2 - i\alpha\hat{\Omega} + \left(2 + \frac{2}{3}\left(\frac{f}{1+f}\right)\right)} \equiv g(\hat{\Omega})\tilde{J}_p. \qquad (51)$$

Combining (49), (50), and (51) results in

$$\left(1 + \zeta\frac{\partial}{\partial\zeta} - fg(\hat{\Omega})\right)\tilde{D} = -\frac{\pi a_o^2}{2c}\left(1+g(\hat{\Omega})\right)\left(1+\zeta\frac{\partial}{\partial\zeta}\right)\sigma_o(r=0)(1-q)\frac{\partial\tilde{D}}{\partial\zeta}. \qquad (52)$$

We have

$$\frac{\pi a_o^2}{2c}\sigma_o(r=0)(1-q) = \lambda_q\zeta^{\frac{1}{1-q}}, \qquad (53)$$

leading to the following sausage growth equation:

$$\left(1 + \zeta\frac{d}{d\zeta} - fg(\hat{\Omega})\right)\tilde{D} = -\lambda_q\left(1+g(\hat{\Omega})\right)\left(1+\zeta\frac{\partial}{\partial\zeta}\right)\zeta^{\frac{1}{1-q}}\frac{d\tilde{D}}{d\zeta}, \qquad (54)$$

with $g(\hat{\Omega})$ defined by (51) and λ_q defined by (53).

C. Numerical Results for Sausage Instability Growth

In this section, numerical solutions to the sausage instability growth equation (54) are presented. The method is similar to that discussed in Sec. II. E. for the hose instability. Figure 6 plots the sausage amplitude $\tilde{D}(\zeta)$ with parameters η_f, λ_o, ζ_N, ζ_o, and f the same as in Fig. 2. The frequency $\hat{\Omega}$ is 1.25 ($\Omega/\Omega_{\beta o} = 0.88$) which is close to the value $\hat{\Omega}_{max}$ for maximum growth, and the damping coefficient in (51) is Lee's suggested value[29] $\alpha = 0.7$. $\hat{\Omega}_{max}$ varies weakly with λ but is strongly dependent on α. Figure 6 shows no sausage instability even for $q = 0.5$ for this case in which f has its nominal value ($f = -0.5$ for $\eta_f = 1$ and $\eta\lambda = 1$).

Lampe and Joyce[28] point out that sausage instability can be generated in the q = 0 limit if η_f exceeds the limit in (46). Figure 7 plots $\tilde{D}(\zeta)$ for a case in which -f has been raised to 0.85 (η_f = 5.67). For q = 0, the beam is very weakly unstable, as expected since η_f is slightly above the threshold given by (46). As q is increased, significant sausage growth appears. The critical of η_f value for the onset of hose instability drops to η_f = 3.2 (f = -0.76) when q = 0.5. Since Sharp and Lampe[22] quote a maximum value of η_f of 3 to 4 in typical beams, this reduction in the threshold for sausage instability may allow beams to be weakly unstable if q is sufficiently large. The hose instability linear amplitudes will be substantially larger, however. Although sausage tends to grow out of perturbations which are larger than those for hose,[28] any experiment which is sausage-unstable is likely to have even more violent hose disruptions.

D. Axi-Symmetric Hollowing Instability

A violent axi-symmetric hollowing instability has been observed in many particle simulations of propagating beams.[15,27,30,31] Joyce and Lampe[15] showed that this instability is driven by avalanche ionization in the high E/ρ region near the front of the beam and proposed that the instability is triggered if $(E/\rho)_{max} > 130$ kV-cm^{-1}-atm^{-1} $\equiv (E/\rho)_{crit}$. Ekdahl et al. have observed violent hollowing instability on the IBEX experiment for beams propagating at pressures of 10-80 torr.[31] Simulations by Godfrey[31] have reproduced the hollowing instability at pressures somewhat above the 80 torr threshold and have confirmed that the instability threshold is close to the Joyce and Lampe[15] prediction.

Although no detailed theory of the avalanche-driven hollowing instability has appeared, the instability is believed to be due to an enhancement of $\sigma(r)$ and $J_p(r)$ near the higher E_z region around the beam

axis. The analysis is complicated by the fact that no Bennett-like equilibrium exists when return current flow near the axis is enhanced, so the simulations appear to be attempting to achieve a new equilibrium at the same time as the instability is being generated.

Simulation studies to date have been made almost exclusively with constant ν_m conductivity models. The inclusion of a $\nu_m(E/\rho)$ model could affect the instability in several ways. Since the instability is triggered in a high E_z region, ν_m and τ_1^{eff} would undoubtedly be smaller for a $\nu_m(E/\rho)$ conductivity model, thus increasing E_{zo} and increasing the growth rate. On the other hand, the radial profile of $\sigma(r)$ would be less peaked on-axis due to the higher $\nu_m(E/\rho)$ near the axis which would tend to increase the threshold for instability. It is not clear which of those effects would dominate. However, since the instability is driven primarily by the strong nonlinearities in the avalanche rate coefficient for $E/\rho \simeq (E/\rho)_{crit}$, it is likely that the variable ν_m effects will not change the threshold significantly. Studies with the SIMMØ particle simulation[15] using the same $\nu_m(E/\rho)$ model[18] contained in the VIPER code do not indicate a significant change in the hollowing instability threshold.[32]

V. CONCLUSIONS

The growth of the resistive hose instability in a relativistic electron beam is strongly dependent upon the details of conductivity generation by the beam. We have considered cases in which beam impact ionization is the dominant conductivity generation mechanism and the collision frequency ν_m is a function of E/ρ, the ratio of the electric field to the neutral gas density. The introduction of variable ν_m introduces two important new features. First, since $\partial\nu_m/\partial(E/\rho) > 0$ for normal weakly ionized gases, and since the electric field usually decreases with distance ζ from the beam head, the local dipole decay length $c\tau_1 = \pi\sigma(r=0)a^2/2c$ tends to be shorter in the front of the beam but longer in the beam tail compared with values usually estimated from constant collision frequency models. As a result, hose amplitudes grow very rapidly near the front of the beam but taper off and approach a constant value in the beam tail. The second feature is a destabilizing effect which is due to localized decreases in the perturbed or dipole conductivity driven by the increase in collision frequency resulting from perturbations in the electric field.

The destabilizing effect is illustrated in Eq. (12) which shows that the term multiplying $\partial A/\partial\zeta$ in Ampere's Law is $(4\pi\sigma_o/c)(1-(E/\nu_m)(\partial\nu_m/\partial E))$. Thus, the beam behaves as if the monopole conductivity σ_o were replaced by $\sigma_o(1-(E/\nu_m)(\partial\nu_m/\partial E)) \equiv \sigma_o(1-\bar{q})$. Since $\bar{q} \gtrsim 0.5$ in some cases, the destabilizing effect can be quite strong. For cases in which $\bar{q}$ is constant and otherwise the assumptions of Ref. 7 are justified, a differential equation for the hose displacement $D(\zeta)$ is derived. Solutions to this equation in terms of confluent hypergeometric functions are given, as are numerical solutions. Plots of $D(\zeta)$ show the pattern of rapid hose growth

followed by a plateau which becomes more pronounced as $\bar{q}$ approaches 1. As $q \to 0$, the $D(\zeta)$ plots approach the pure power law behavior described in Ref. 7.

Simulations of hose instability growth using the VIPER[7] model allow a more self-consistent treatment. In this model, the monopole and dipole beam and net current densities, etc. can vary with ζ and propagation distance z. The two major features of variable collision frequency described above are observed in the simulations and, in fact, were noticed in simulations before the analytical models were obtained.

Variations in momentum transfer frequency can also affect the sausage instability. We have extended earlier calculations of Lampe and Joyce[28] to include these effects and find that although variable ν_m dipole conductivity effects lower the threshold for instability, strong sausage instability growth is unlikely except in extreme cases. Such cases would be violently hose unstable as well.

REFERENCES

1. J. C. Clark, K. W. Struve, S. S. Yu and R. E. Melendex, Proc. Fifth Intl. Conf. on High-Power Particle Beams (R.J. Briggs, A.J. Toepfer, eds.), San Francisco, 1983, p. 412.

2. R. J. Adler, G. F. Kiuttu and B. Sabol, Proc. Fifth Intl. Conf. on High-Power Particle Beams(R.I. Briggs, A.J. Toepfer, eds.), San Francisco, 1983, p. 366.

3. D. P. Murphy, M. Raleigh, R. E. Pechacek and J. R. Greig, Proc. Fifth Intl. Conf. on High Power Particle Beams (R. Briggs, A. Toepfer, eds.), San Francisco, 1983, p. 389.

4. R. J. Briggs, J. C. Clark, T. J. Fessenden, R. E. Hester and E. J. Lauer, Proc. of the 2nd Intl. Topical Conf. on High Power Electron Beam Research and Technology (Cornell Univ., Ithaca, NY, 1977) Vol. I, p. 319.

5. E. P. Lee, Phys. Fluids 21, 1327 (1978).

6. W. M. Sharp, M. Lampe and H. S. Uhm, Phys. Fluids 25, 1456 (1982).

7. M. Lampe, W. Sharp, R. F. Hubbard, E. P. Lee and R. J. Briggs, Phys. Fluids 27, 2921 (1984).

8. E. P. Lee, F. W. Chambers, L. L. Lodestro and S. S. Yu, Proc. of the 2nd Intl. Topical Conf. on High Power Electron Beam Research and Technology (Cornell Univ., Ithaca, NY, 1977) Vol. I, p. 381.

9. W. Fawley and W. Sharp (unpublished); W. Fawley and E. P. Lee (unpublished).

10. G. Joyce and M. Lampe, J. Comp. Phys. 63, 398 (1986).

11. R. L. Feinstein, D. A. Keeley, E. R. Parkinson and W. Reinstra, Science Applications International Corp. Report SAIC-U-74-PA-DOE (1984).

12. B. B. Godfrey and D. Mitrovitch (unpublished).

13. S. Slinker, R. Hubbard, R. Fernsler, A. W. Ali and M. Lampe, "Effects of Temperature-Dependent Conductivity on Hose", contained in NRL Memo Report 5412 (1984).

14. R. F. Hubbard, G. Joyce, S. P. Slinker, M. Lampe and J. M. Picone, Bull. Am. Phys. Soc. 30, 1583 (1985).

15. G. Joyce and M. Lampe, Phys. Fluids 26, 3377 (1983).

16. H. Massey, Atomic and Molecular Collisions, (Wiley, NY), 1979.

17. S. P. Slinker and A. W. Ali, Naval Research Laboratory Memorandum Report 5614 (1985). ADA157030

18. S. P. Slinker and R. F. Hubbard, Naval Research Laboratory Memorandum Report 5777 (1986). ADA167134

19. E. H. Holt and R. E. Haskell, "Plasma Dynamics", MacMillen, New York, 1965, p. 288.

20. P. Felsenthal and J. M. Proud, Phys. Rev. 139, A1796 (1965).

21. A. W. Ali, Naval Research Laboratory Memorandum Report 4794 (1982). ADA113501

22. W. M. Sharp and M. Lampe, Phys. Fluids 23, 2383 (1980).

23. E. P. Lee, Phys. Fluids 19, 60 (1976).

24. R. J. Briggs, R. E. Hester, W. A. Lamb, E. J. Lauer and R. L. Spoerlein, Bull. Am. Phys. Soc. 19, 902 (1974).

25. M. Abramowitz and I. A. Stegun, Handbook of Mathematical Functions, (Dover Publications, NY), 1965, p. 504.

26. L. G. Christophorou, S. R. Hunter, J. G. Carter and R. A. Mathis, Appl. Phys. Lett. 41 147 (1982).

27. M. Lampe, G. Joyce and R. F. Hubbard, Proc. of the Fifth Intl. Conf. on High-Power Particle Beams(R. J. Briggs, A. J. Toepfer, eds.), San Francisco, 1983, p. 336.

28. M. Lampe and G. Joyce, Phys. Fluids 26, 3371 (1983).

29. E. P. Lee, Lawrence Livermore Laboratory Report UCID-18940 (1981). E. P. Lee and S. S. Yu, Lawrence Livermore Laboratory Report UCID 18330 (1979).

30. K. Brueckner (unpublished); F. Chambers (unpublished).

31. C. A. Ekdahl, J. R. Freeman, G. T. Leifeste, R. B. Miller, W. B. Stygar and B. B. Godfrey, Phys. Rev. Lett. 55, 935 (1985).

32. G. Joyce, S. P. Slinker and R. Hubbard (unpublished).

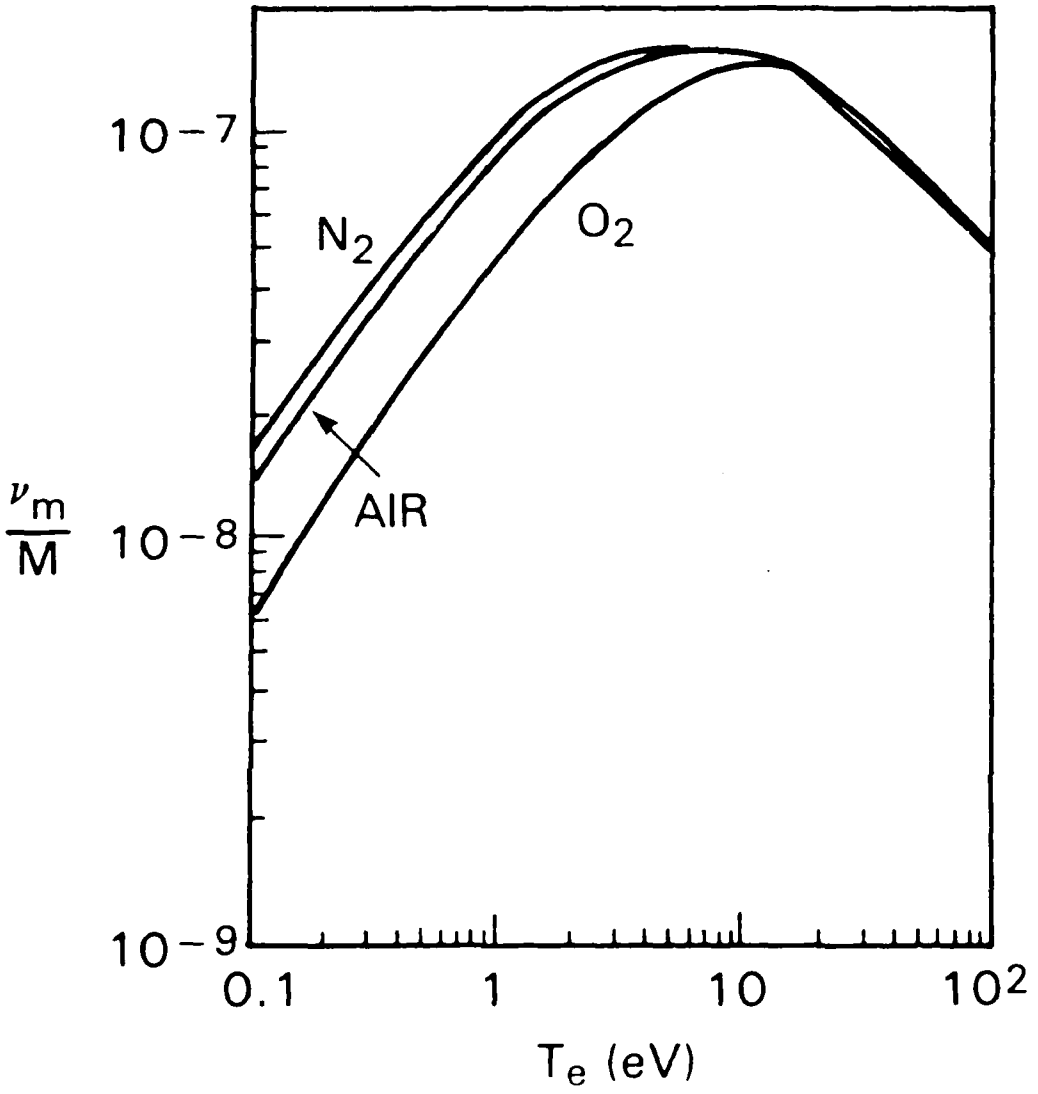

Fig. 1 ν_m/M (cm^3/sec) for N_2, O_2 and air. (Ref. 17).

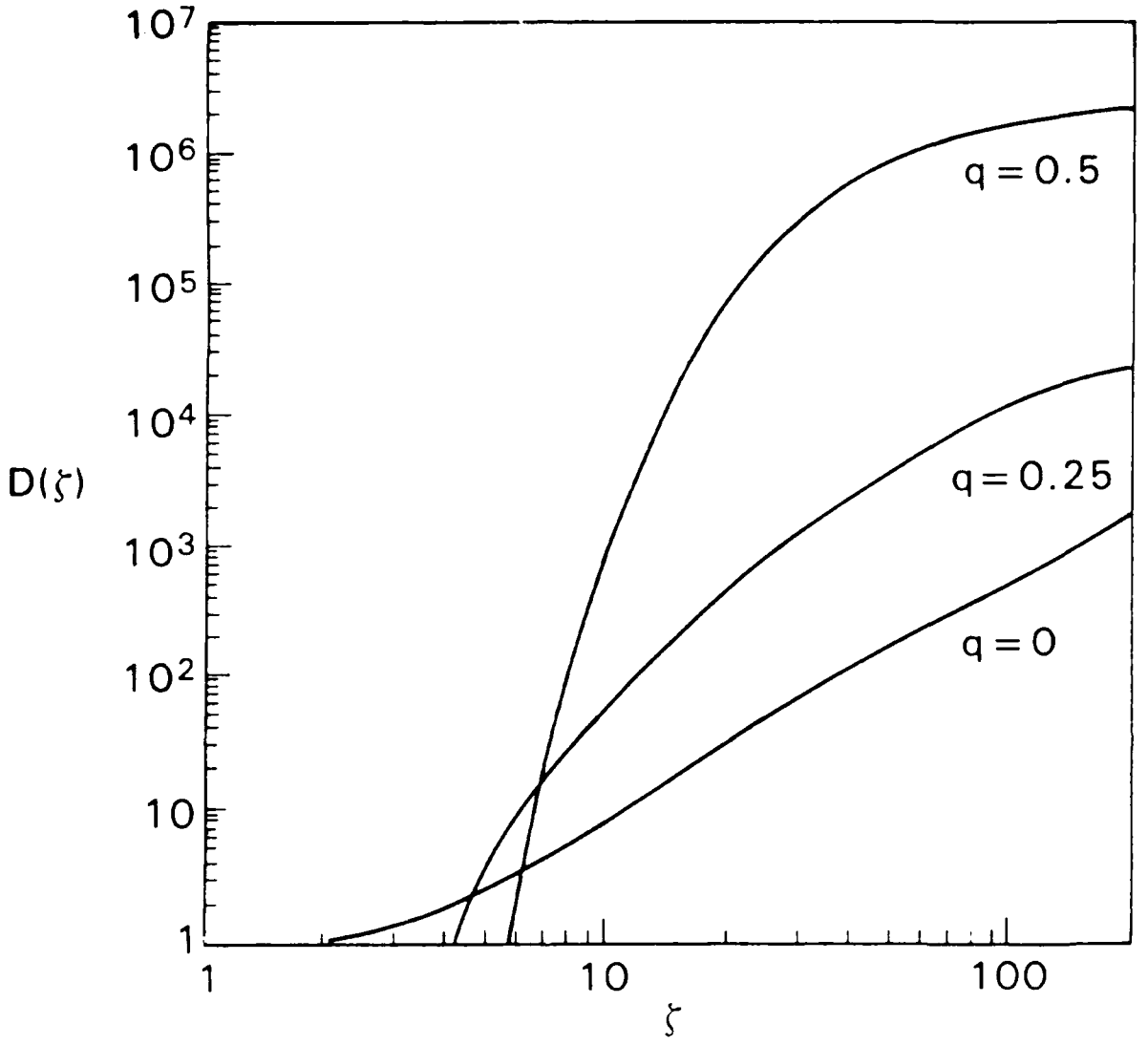

Fig. 2 Hose instability growth for various values of q. Solutions obtained from Eq. (28), assuming $\eta_f = \lambda_o = 1$, $\zeta_N = 20a_o$, $f = -0.5$, $\Omega_r/\Omega_{\beta o} = 0.5$, and $c\tau_1(\zeta_o) = a_o$.

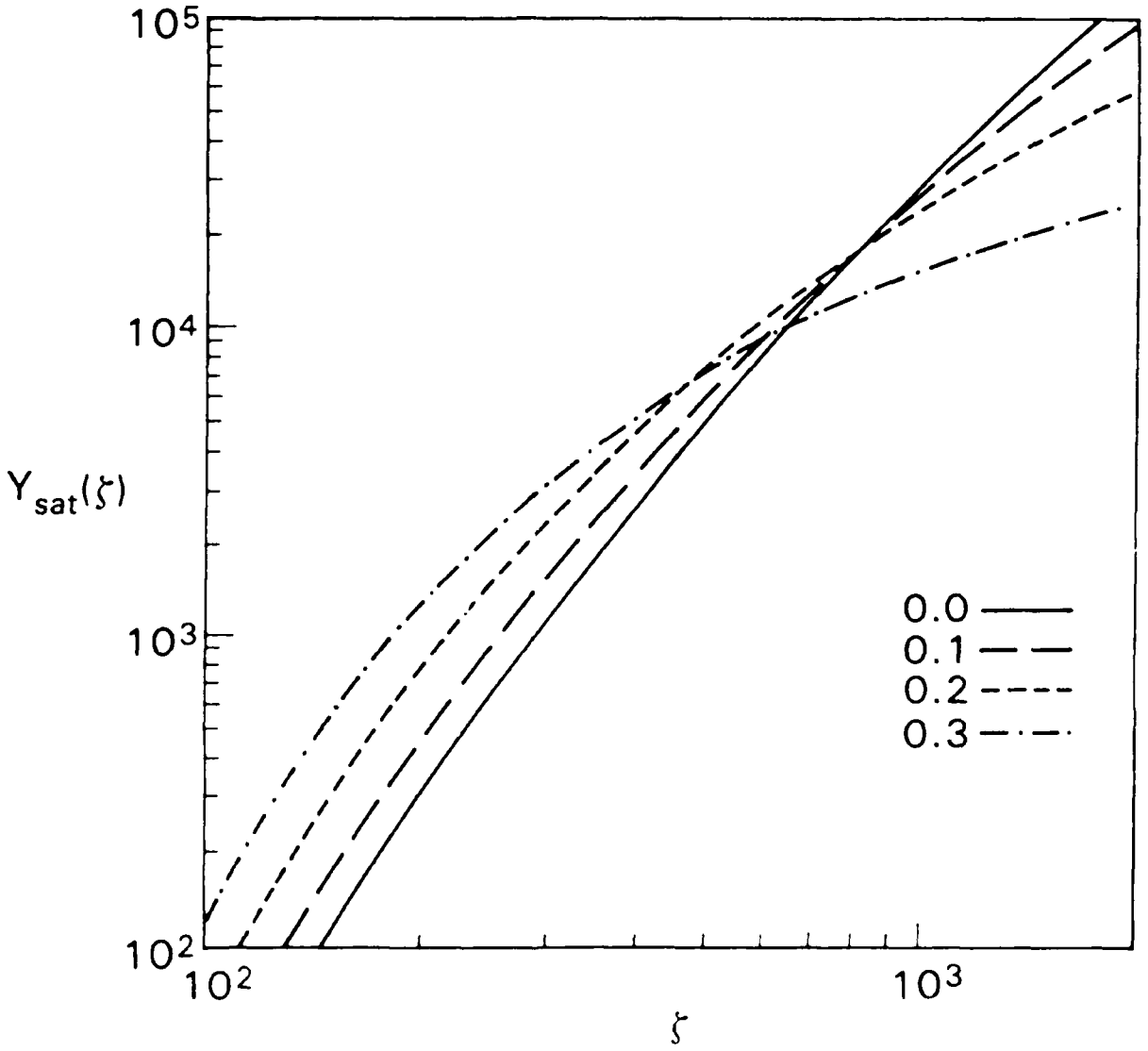

Fig. 3 Saturated hose amplitude for q = 0, 0.1, 0.2 and 0.3. Results obtained from VIPER simulations.

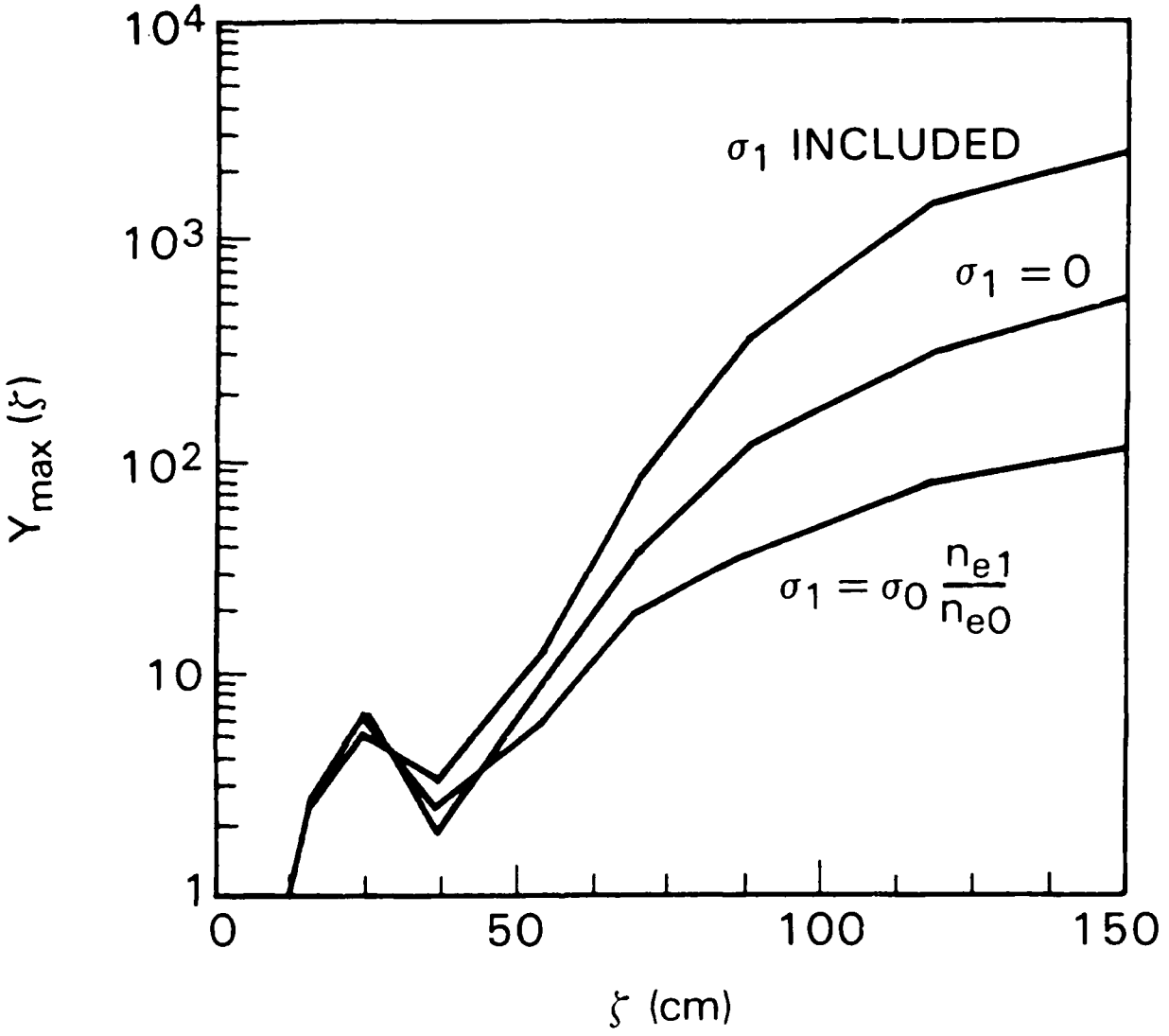

Fig. 4 VIPER simulations showing the effects of dipole conductivity on hose instability growth. Case A has all the σ_1 terms included (Eq. 9b). Case B has $\sigma_1 = 0$. Case C has only the direct production contribution to σ_1:

$$\sigma_1 = \sigma_o \frac{n_{e1}}{n_{eo}} .$$

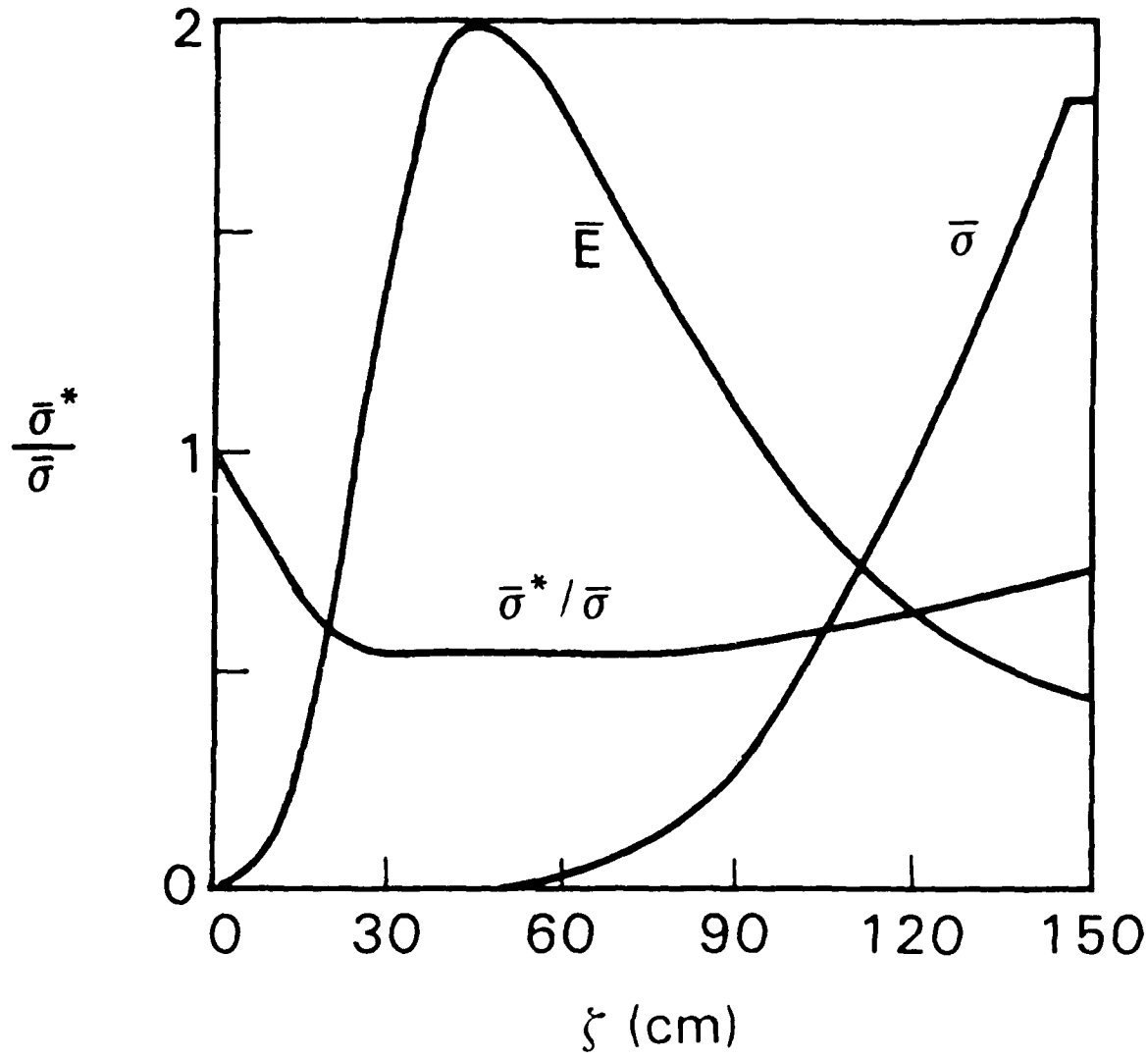

Fig. 5 On-axis electric field $\bar{E}$ (arbitrary units), on-axis conductivity $\bar{\sigma}$ (arbitrary units) and fraction $\bar{\sigma}^*/\bar{\sigma}$ (left-hand scale). Data from Case A of Fig. 4.

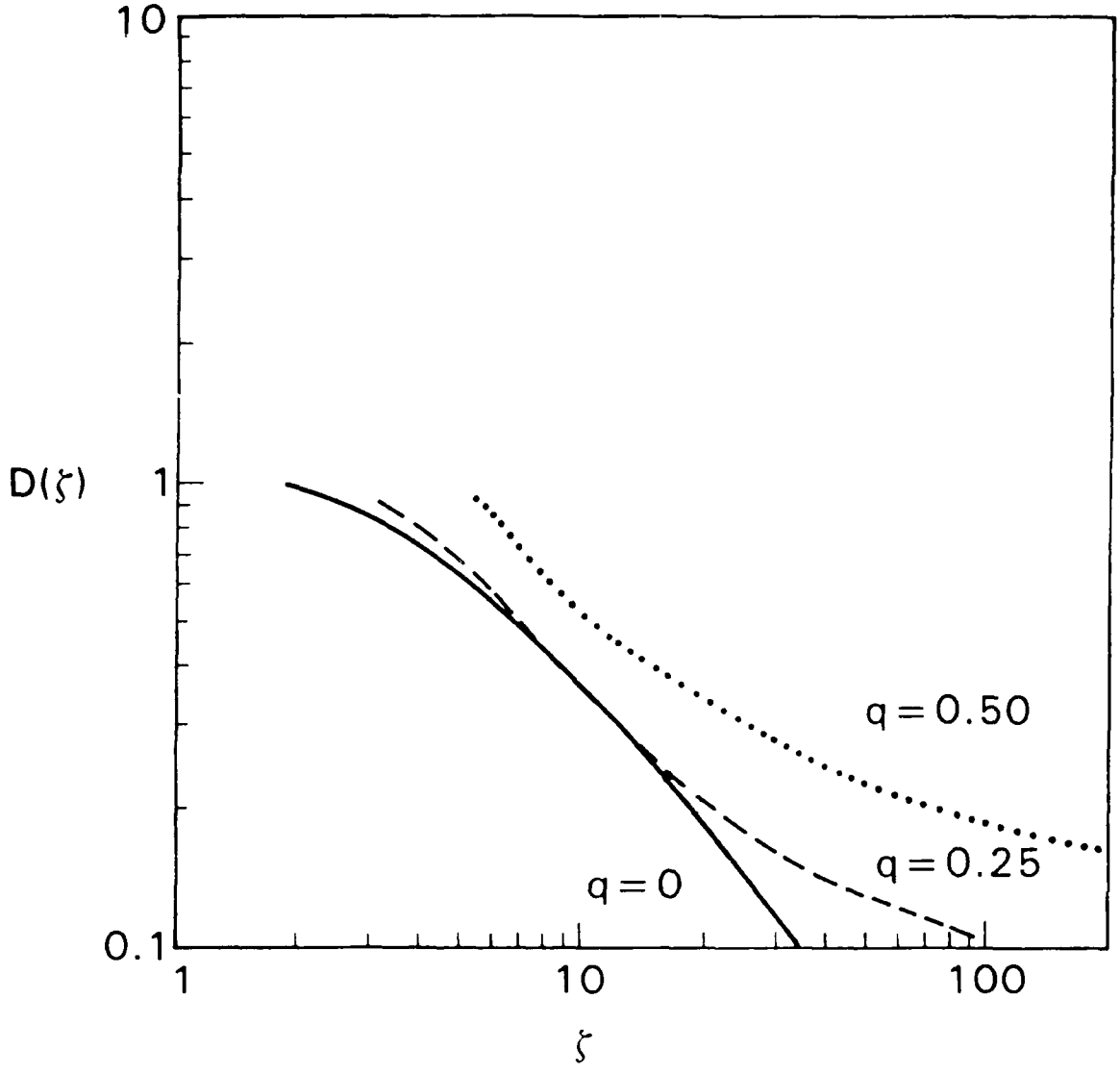

Fig. 6 Sausage instability growth for various values of q. Solutions obtained from Eq. (54), with η_f, λ_o, ζ_N, ζ_o, and f as in Fig. 2.

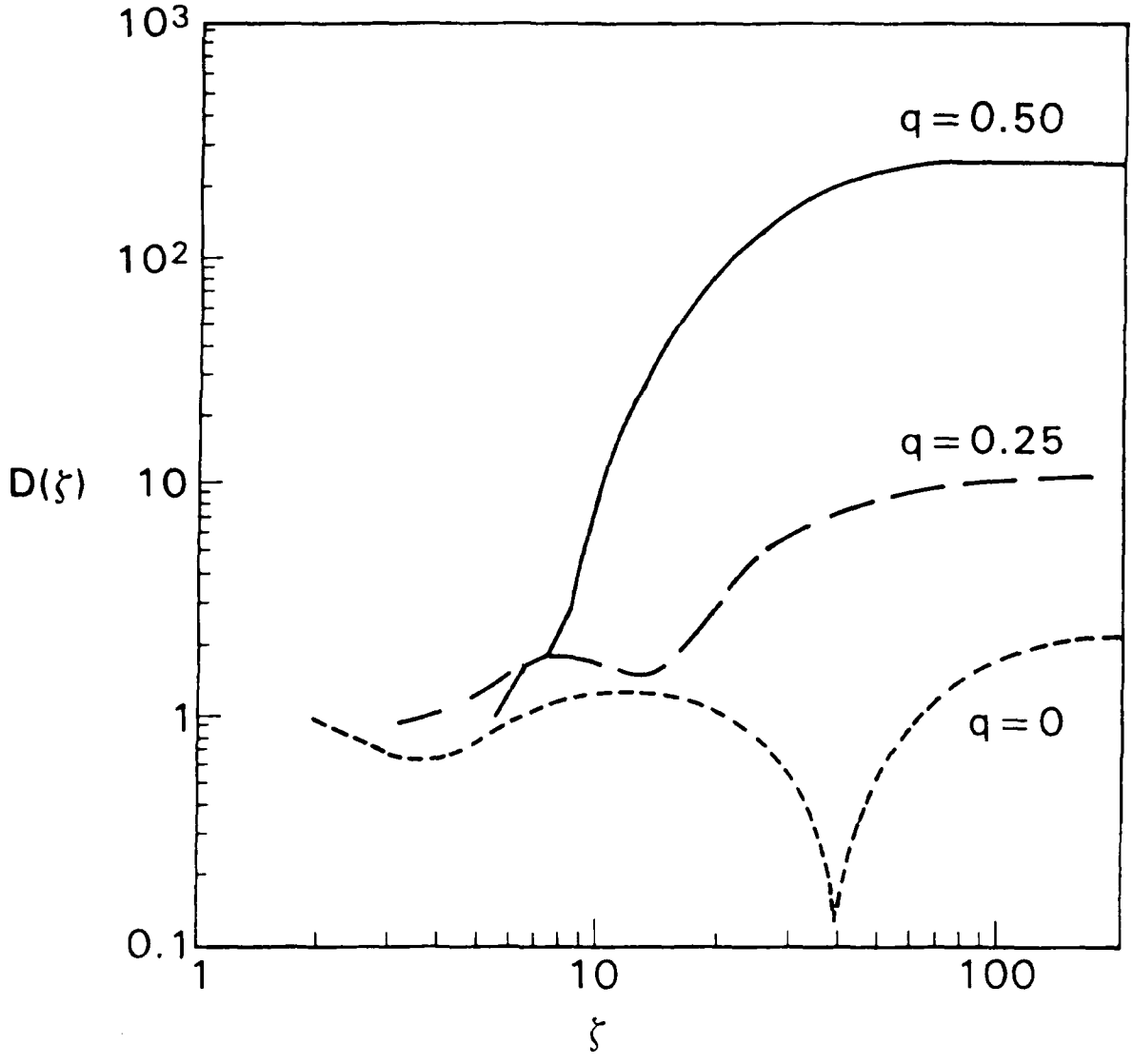

Fig. 7 Sausage instability growth for various values of q. In this case, the current neutralization fraction is set to f = -.85, and other parameters are the same as in Fig. 6.

Distribution List

Naval Research Laboratory
4555 Overlook Avenue, S.W.
Washington, D.C. 20375-5000

Attn: Dr. M. Lampe - Code 4792 (30 copies)
Dr. T. Coffey - Code 1001
Dr. J. Boris - Code 4040
Dr. M. Picone - Code 4040
Dr. J. B. Aviles - Code 4665
Dr. M. Haftel - Code 4665
Dr. S. Ossakow - Code 4700 (26 copies)
Dr. A. Ali - Code 4700.1
Dr. M. Friedman - Code 4700.1
Dr. R. Taylor - BRA (4700.1)
Mr. I. M. Vitkovitsky - Code 4701
Dr. S. Gold - Code 4740
Dr. A. Robson - Code 4760
Dr. M. Raleigh - Code 4760
Dr. R. Meger - Code 4763
Dr. D. Murphy - Code 4763
Dr. R. Pechacek - Code 4763
Dr. G. Cooperstein - Code 4770
Dr. D. Colombant - Code 4790
Dr. R. Fernsler - Code 4790
Dr. I. Haber - Code 4790
Dr. R. F. Hubbard - Code 4790 (30 copies)
Dr. G. Joyce - Code 4790
Dr. Y. Lau - Code 4790
Dr. S. P. Slinker - Code 4790 (30 copies)
Dr. P. Sprangle - Code 4790
Code 4790 (20 copies)
Library - Code 2628 (20 copies)
D. Wilbanks - Code 2634
Code 1220

Air Force Office of Scientific Research
Physical and Geophysical Sciences
Bolling Air Force Base
Washington, DC 20332
Attn: Major Bruce Smith

Air Force Weapons Laboratory
Kirtland Air Force Base
Albuquerque, NM 87117
Attn: W. Baker (AFWL/NTYP)
D. Dietz (AFWL/NTYP)
Lt Col J. Head

U. S. Army Ballistics Research Laboratory
Aberdeen Proving Ground, Maryland 21005
Attn: Dr. Donald Eccleshall (DRXBR-BM)
Dr. Anand Prakash

Avco Everett Research Laboratory
2385 Revere Beach Pkwy
Everett, Massachusetts 02149
Attn: Dr. R. Patrick
Dr. Dennis Reilly

Ballistic Missile Def. Ad. Tech. Ctr.
P.O. Box 1500
Huntsville, Alabama 35807
Attn: Dr. M. Hawie (BMDSATC-1)

Chief of Naval Material
Office of Naval Technology
MAT-0712, Room 503
800 North Quincy Street
Arlington, VA 22217
Attn: Dr. Eli Zimet

Cornell University
369 Upson Hall
Ithaca, NY 14853
Attn: Prof. David Hammer

DASIAC - DETIR
Kaman Tempo
25600 Huntington Avenue, Suite 500
Alexandria, VA 22303
Attn: Mr. F. Wimenitz

Defense Advanced Research Projects Agency
1400 Wilson Blvd.
Arlington, VA 22209
Attn: Dr. Shen Shey
Dr. H. L. Buchanan

Department of Energy
Washington, DC 20545
Attn: Dr. Wilmot Hess (ER20:GTN,
High Energy and Nuclear Physics)
Mr. Gerald J. Peters (G-256)

Directed Technologies, Inc.
226 Potomac School Road
McLean, VA 22101
Attn: Dr. Ira F. Kuhn
Dr. Nancy Chesser

C. S. Draper Laboratories
555 Technology Square
Cambridge, Massachusetts 02139
Attn: Dr. E. Olsson
Dr. L. Matson

Institute for Fusion Studies
University of Texas at Austin
RLM 11.218
Austin, TX 78712
Attn: Prof. Marshall N. Rosenbluth

Intelcom Rad Tech.
P.O. Box 81087
San Diego, California 92138
Attn: Dr. W. Selph

Joint Institute for Laboratory
Astrophysics
National Bureau of Standards and
University of Colorado
Boulder, CO 80309
Attn: Dr. Arthur V. Phelps

Kaman Sciences
1500 Garden of the Gods Road
Colorado Springs, CO 80933
Attn: Dr. John P. Jackson

Lawrence Berkeley Laboratory
University of California
Berkeley, CA 94720
Attn: Dr. Edward P. Lee

Lavrence Livermore National Laboratory
University of California
Livermore, California 94550
Attn: Dr. Richard J. Briggs
Dr. Simon S. Yu
Dr. Frank Chambers
Dr. James W.-K. Mark, L-477
Dr. William Fawley
Dr. William Barletta
Dr. William Sharp
Dr. Daniel S. Prono
Dr. John K. Boyd
Dr. Kenneth W. Struve
Dr. John Clark
Dr. George J. Caporaso
Dr. William E. Martin
Dr. Donald Prosnitz

Lockheed Missiles and Space Co.
3251 Hanover St.
Bldg. 205, Dept 92-20
Palo Alto, CA 94304
Attn: Dr. John Siambis

Los Alamos National Scientific Laboratory
P.O. Box 1663
Los Alamos, NM 87545
Attn: Dr. L. Thode
Dr. M. A. Mostrom, MS-608
Dr. H. Dogliani, MS-5000
Dr. R. Carlson
Ms. Leah Baker, MS-P940
Dr. Carl Ekdahl

Maxwell Laboratories Inc.
8888 Balboa Avenue
San Diego, CA 92123
Attn: Dr. Ken Whitham

McDonnell Douglas Research Laboratories
Dept. 223, Bldg. 33, Level 45
Box 516
St. Louis, MO 63166
Attn: Dr. Evan Rose
Dr. Carl Leader

Mission Research Corporation
EM Systems Applications
1720 Randolph Road, S.E.
Albuquerque, NM 87106
Attn: Dr. Brendan Godfrey
Dr. Thomas Hughes
Dr. Lawrence Wright
Dr. A. B. Newberger

Mission Research Corporation
P. O. Drawer 719
Santa Barbara, California 93102
Attn: Dr. C. Longmire
Dr. N. Carron

National Bureau of Standards
Gaithersburg, Maryland 20760
Attn: Dr. Mark Wilson

Naval Surface Weapons Center
White Oak Laboratory
Silver Spring, Maryland 20903-5000
Attn: Dr. R. Cawley
Dr. J. W. Forbes
Dr. B. Hui
Mr. W. M. Hinckley
Mr. N. E. Scofield
Dr. E. C. Whitman
Dr. M. H. Cha
Dr. H. S. Uhm
Dr. R. Fiorito
Dr. K. T. Nguyen
Dr. R. Stark
Dr. R. Chen

Office of Naval Research
800 North Quincy Street
Arlington, VA 22217
Attn: Dr. C. W. Roberson
Dr. M. Moss

Office of Naval Research (2 copies)
Department of the Navy
Code 01231C
Arlington, VA 22217

Office of Under Secretary of Defense
Research and Engineering
Room 3E1034
The Pentagon
Washington, DC 20301
Attn: Mr. John M. Bachkosky

ORI, Inc.
1375 Piccard Drive
Rockville, MD 20850
Attn: Dr. C. M. Huddleston

Physical Dynamics, Inc.
P.O. Box 1883
La Jolla, California 92038
Attn: Dr. K. Brueckner

Physics International, Inc.
2700 Merced Street
San Leandro, CA. 94577
Attn: Dr. E. Goldman

Princeton University
Plasma Physics Laboratory
Princeton, NJ 08540
Attn: Dr. Francis Perkins, Jr.

Pulse Sciences, Inc.
600 McCormack Street
San Leandro, CA 94577
Attn: Dr. Sidney Putnam
Dr. John Bayless

Sandia National Laboratory
Albuquerque, NM 87115
Attn: Dr. Bruce Miller
Dr. Collins Clark
Dr. Barbara Epstein
Dr. John Freeman
Dr. Charles Frost
Dr. Gordon T. Leifeste
Dr. Gerald N. Hays
Dr. James Chang
Dr. Michael G. Mazerakis
Dr. John Wagner
Dr. Ron Lipinski

Science Applications Intl. Corp.
P. O. Box 2351
La Jolla, CA 92038
Attn: Dr. Rang Tsang

Science Applications Intl. Corp.
5150 El Camino Road
Los Altos, CA 94022
Attn: Dr. R. R. Johnston
Dr. Leon Feinstein
Dr. Douglas Keeley

Science Applications Intl. Corp.
1710 Goodridge Drive
McLean, VA 22102
Attn: Mr. W. Chadsey
Dr. A Drobot
Dr. K. Papadopoulos
Dr. B. Hui

Commander
Space & Naval Warfare Systems Command
PMW-145
Washington, DC 20363-5100
Attn: CAPT J. D. Fontana
CDR W. Bassett

SRI International
PS0-15
Molecular Physics Laboratory
333 Ravenswood Avenue
Menlo Park, CA 94025
Attn: Dr. Donald Eckstrom

Strategic Defense Initiative Org.
1717 H Street, N. W.
Washington, DC 20009
Attn: Lt Col R. L. Gullickson
Dr. J. Ionson
Dr. D. Duston

Strategic Defense Initiative Office
Directed Energy Weapons Office, The Pentagon
Office of the Secretary of Defense
Washington, DC 20301-7100
Attn: Dr. C. F. Sharn (OP0987B)

Titan Systems, Inc.
9191 Towne Centre Dr.-Suite 500
San Diego, CA 92122
Attn: Dr. R. M. Dowe

University of California
Physics Department
Irvine, CA 92664
Attn: Dr. Gregory Benford

University of Maryland
Physics Department
College Park, MD 20742
Attn: Dr. Y. C. Lee
Dr. C. Grebogi

University of Michigan
Dept. of Nuclear Engineering
Ann Arbor, MI 48109
Attn: Prof. Terry Kammash
Prof. R. Gilgenbach

Director of Research
U.S. Naval Academy
Annapolis, MD 21402 (2 copies)

DEPARTMENT OF THE NAVY

NAVAL RESEARCH LABORATORY
Washington, D C 20375-5000

OFFICIAL BUSINESS
PENALTY FOR PRIVATE USE, $300

THIRD-CLASS MAIL
POSTAGE & FEES PAID
USN
PERMIT No. G-9